Phase transition of surface models with intrinsic curvature

H. Koibuchi[a], N. Kusano, A. Nidaira, Z. Sasaki, and K. Suzuki

Department of Mechanical and Systems Engineering, Ibaraki College of Technology, Nakane 866, Hitachinaka, Ibaraki 312-8508, Japan

Abstract. It is reported that a surface model of Polyakov strings undergoes a first-order phase transition between smooth and crumpled (or branched polymer) phases. The Hamiltonian of the model contains the Gaussian term and a deficit angle term corresponding to the weight of the integration measure dX in the partition function.

PACS. 64.60.-i General studies of phase transitions – 68.60.-p Physical properties of thin films, nonelectronic – 87.16.Dg Membranes, bilayers, and vesicles

1 Introduction

A large effort has been devoted to the understanding of the phase structure of elastic membrane models of Polyakov-Kleinert [1,2] and Helfrich [3]. The surface models are expected to undergo phase transitions between smooth and crumpled phases at finite bending rigidity [4–14]. Numerical studies have also been concentrated on the phase transition [15–24].

The bending energy, which is an extrinsic curvature term, plays an essential role in smoothing the surface. In the ordinary model of membranes, the smooth phase emerges owing to the bending energy. Except self-avoiding surface models [25–29], we have currently no surface model that has a smooth phase without the extrinsic curvature term.

Baillie-Johnston et al. [30–33] investigated the discretized Polyakov random surface model with intrinsic curvature terms in order to find smooth surfaces. One of the models was recently investigated in [34] on relatively larger lattices, however, there was no smooth phase in the model, although branched polymer like phase was found. We consider that the question about a smooth phase in the models remains unanswered, and the surface model with intrinsic curvatures remains to be studied. Thus, motivated by the attempts of Baillie-Jhonston et al., we study in this article a model with an intrinsic curvature term and see that the smooth phase and the crumpled phase are appeared and connected by a phase transition. Our results may lead to better understanding of the role of curvature energy in surface models undergoing phase transitions and/or shape transformation, although the surfaces are allowed to self-intersect and hence phantom.

Two kinds of models are investigated; the tethered model and the fluid model. The tethered model is defined on fixed connectivity surfaces, and the fluid model on dynamically triangulated surfaces. The Hamiltonians of the models are identical with each other. It will be shown that the tethered model has the smooth and the crumpled phases, which are connected by a first-order phase transition. Moreover, we will find in the fluid model that there appears a new phase, which resembles the branched polymer phase [35,36], between the smooth phase and the crumpled one. We understand from the results obtained in this article that the smooth phase is stable against such as thermal fluctuations in each model defined only with intrinsic variables of the surface.

2 Model

The partition function of the fluid model of fixed number of vertices is defined by

$$Z = \sum_{\mathcal{T}} \int \prod_{i=1}^{N} dX_i \exp\left[-S(X, \mathcal{T})\right], \qquad (1)$$
$$S(X, \mathcal{T}) = S_1 - \alpha S_3,$$

where the center of the surface is fixed to remove the translational zero mode. $S(X, \mathcal{T})$ denotes that the Hamiltonian S depends on the position variables X of vertices and the degree of freedom for the triangulation $\mathcal{T}$. S_1 and S_3 are defined by

$$S_1 = \sum_{(ij)} (X_i - X_j)^2, \quad S_3 = \sum_i \log(\delta_i/2\pi), \quad (2)$$

where $\sum_{(ij)}$ in S_1 is the sum over bonds (ij) connecting the vertices i and j. The bonds (ij) are edges of the

[a] e-mail: koibuchi@mech.ibaraki-ct.ac.jp

triangles. δ_i in equation (2) is the vertex angle, which is the sum of the angles meeting at the vertex i. Recalling that $\delta_i - 2\pi$ is the deficit angle, we call S_3 the deficit angle term. We note that the sum of the deficit angles $\sum_i(\delta_i - 2\pi)$ is constant on surfaces of fixed genus because of the Gauss-Bonnet theorem. The partition function of the tethered model is, on the other hand, defined by $Z = \int \prod_{i=1}^{N} dX_i \exp\left[-S(X, \mathcal{T})\right]$, where $\mathcal{T}$ is fixed. Both S_1 and S_3 reflect intrinsic properties of the surface. Note also that $S_1/N = 3/2$, which comes from the scale invariance property of Z in both models.

We should refer to a relation between the deficit angle term S_3 and the integration measure dX_i of the partition function in equation (1). From a conformal field theoretical viewpoint [37–40], the integration measure $\prod_i dX_i$ can be replaced by $\prod_i q_i^\alpha dX_i$, where q_i is the coordination number of the vertex i. This α is believed to be $2\alpha = 3$. On the other hand, q_i^α is considered as a volume weight of the vertex i in the measure dX_i. Hence, it is possible to extend 2α to non-integer numbers by assuming that the weight can be chosen arbitrarily. Moreover, it is also possible to extend q_i to continuous numbers because of the same reason. Hence, the weight $\prod_i q_i^\alpha$ can be replaced by $\prod_i \delta_i^\alpha$, which can also be written as $\exp(\alpha \sum_i \log \delta_i)$. Including a constant weight $(2\pi)^\alpha$, we have S_3 in equation (2).

The model in this paper is very similar to the one investigated in [30–34], where the fluid and the tethered models were interpolated. A model in [30–34] includes the term $\alpha \sum_i |q_i - 6|$ or $\alpha \sum_i (q_i - 6)^2$. Using the expression $\log(\delta_i/2\pi) = \log[1 + (\delta_i - 2\pi)/2\pi]$ and replacing δ_i by q_i and 2π by 6 in S_3 of equation (2), we have the term proportional to $\sum_i (q_i - 6)^2$ + (higher order). Thus, we confirmed that the lowest order term in S_3 is identical with the expression $\alpha \sum_i (q_i - 6)^2$ described above upto multiplicative constant. We note that the similarity between S_3 of equation (2) and a deficit angle term denoted by S_{tight} in [30] can also be seen.

We will see below that the fluid surfaces become crumpled, branched polymer like, and smooth, when α increases from $\alpha = 0$. A higher-order transition separates the branched polymer phase from the crumpled one, and a first-order transition separates the branched polymer phase from the smooth one. On the other hand, we find in [34] that the fluid surfaces become crumpled, branched polymer, and crumpled, with increasing α. One of the transitions is of higher (or second) order, and the other is of first order, in the model of [34].

It should also be noted on differences between $S_3(\delta)$ of equation (2) and the corresponding term $S_3(q) = \sum_i \log(q_i/6)$, which can be expanded to $\sum_i (q_i - 6)^2$ + (higher order) as described above. Although the difference between these two S_3 comes only from the one between q and δ, the roles of q and δ in the model make large differences in the results. A major difference between the fluid model in this paper and the one in [34] is whether the model has a smooth phase or not. q is unchanged in the MC update of X, whereas δ changes in that process. As a consequence, while the coordination dependent term $S_3(q)$ is non-trivial only in the fluid model, $S_3(\delta)$ in equation (2) is non-trivial both in the tethered and in the fluid models. In fact, the model with $\sum_i(q_i-6)^2$ has no smooth phase [34], whereas the model with $S_3(\delta)$ in equation (2) has the smooth phase both in the tethered and in the fluid surfaces as we will see below.

3 Monte Carlo simulations

The spherical surfaces, the starting configurations of MC for the fluid model, are discretized by the Voronoi triangulation [41] in $\mathbf{R}^3$. The radii of the initial spheres are chosen so that $S_1/N \simeq 3/2$. The surfaces are constructed relatively uniform in coordination number; the maximum coordination number is about 8.

On the contrary, the uniform lattices, on which the tethered model is defined, were obtained by MC with dynamical triangulation for a model defined by $S = S_1 + bS_2 - \alpha \sum_i \log(q_i/6)$, where $S_2 = \sum_i(1 - \cos\theta_i)$ is the bending energy. Using the parameters $\alpha = 280$, $b = 2$ (or $\alpha = 350$, $b = 2$), we obtained the uniform lattices. By monitoring the number N_5 of vertices of $q_i = 5$, we stopped the MC run when N_5 first reduced to 12, and thus obtained the uniform lattices. The uniform lattices, which will be utilized in simulations for the tethered model, are thus characterized by $N_5 = 12$ and $N_6 = 3N - 18$. In each lattice, only 12 vertices are of $q_i = 5$, and all other vertices are of $q_i = 6$. Except the lattices of $N_5 = 12$, there exists no lattice whose q_i are of $q_i = 5$ or $q_i = 6$. This is easily understood from the fact that $N_B = 3N - 6$ on triangulated surfaces of spherical topology, where N_B is the total number of bonds.

The canonical Metropolis MC technique is used to update the variables X and $\mathcal{T}$. In the MC simulations, the new position of X is chosen so that $X' = X + \delta X$, where δX takes value randomly in a small sphere. The radius δr of the small sphere is defined by using a constant number ϵ as an input parameter so that

$$\delta r = \epsilon \langle l \rangle, \tag{3}$$

where $\langle l \rangle$ is the mean bond length computed at every 250 MCS (Monte Carlo sweeps), and $\langle l \rangle$ is constant in the equilibrium configurations because $S_1/N = 3/2$. The new position X' is accepted with the probability $\text{Min}[1, \exp(-\Delta S)]$, where $\Delta S = S(\text{new}) - S(\text{old})$. The parameter ϵ in equation (3) is chosen to maintain about $50\% \sim 60\%$ acceptance for X. A lower bound $10^{-6} \times A_0$ is assumed for the area of triangles, where A_0 is the mean area of triangles evaluated at every 250 MCS. X' is generated so that the resulting areas of triangles are larger than $10^{-6} \times A_0$. It should be emphasized that the results obtained by using δr in equation (3) are identical with those by using a constant δr.

The triangulation $\mathcal{T}$ is updated by the bond flip. Then, the acceptance rate $r_{\mathcal{T}}$ for the bond flip is uncontrollable. We have, in our MC simulations, $15\% \leq r_{\mathcal{T}} \leq 35\%$, and find that $r_{\mathcal{T}}$ discontinuously changes at a discontinuous transition which will be shown below.
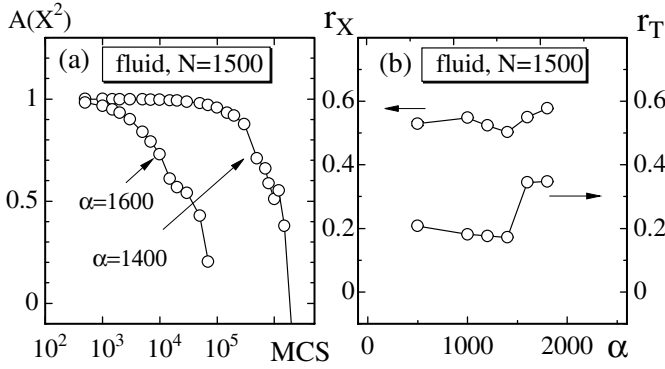
Fig. 1. (a) $A(X^2)$ at $\alpha = 1400$ and at $\alpha = 1600$ on $N = 1500$ fluid surface, and (b) the acceptance rates r_X for X and r_T for $\mathcal{T}$ of the fluid surface model.

The bond is flipped so that the resulting areas of triangles are larger than $10^{-6} \times A_0$ as in the process for X. No restriction is imposed on the bond length in the update of the variables X and $\mathcal{T}$. The maximum coordination number $q_i^{\max}$ of the fluid surface of size $N = 1500$ was about $q_i^{\max} \simeq 20$ both in the smooth phase and in the branched polymer phase, and $q_i^{\max} \simeq 30$ in the crumpled phase. The histogram $h(q)$ of the coordination number q will be shown below. N-trials for X and N-trials for $\mathcal{T}$ make one MCS in the fluid model.

The canonical ensemble average $\langle Q \rangle$ is computed via the time series average of a series $\{Q_i\}$. A series $\{Q_i\}$ is sampled at every 500 MCS after thermalization sweeps, which are large enough so that the mean square size X^2, defined by

$$X^2 = \frac{1}{N} \sum_i \left(X_i - \bar{X} \right)^2, \qquad \bar{X} = \frac{1}{N} \sum_i X_i, \quad (4)$$

becomes statistically independent from the starting configurations. In fact, 0.5×10^7 MCS are discarded for the thermalization of surfaces of $N \leq 600$, and 1×10^7 MCS for $N \geq 1000$ surfaces. Total number of MCS is about $(8 \sim 10) \times 10^7$ at the vicinity of the transition point of $N \geq 1000$ fluid model and of $N \geq 1500$ tethered model, and it is relatively smaller in other cases.

The model membrane is expected to swell out at large α and crumple at small α. Therefore, the shape of membrane, which is an extrinsic property of surfaces, is characterized by X^2. In order to see the correlation in the series of X^2, the autocorrelation coefficient

$$A(X^2) = \frac{\sum_i X^2(\tau_i) X^2(\tau_{i+1})}{\left[\sum_i X^2(\tau_i) \right]^2}, \quad (5)$$
$$\tau_{i+1} = \tau_i + n \times 500, \quad n = 1, 2, \cdots$$

is plotted in Figure 1a, where $X^2(\tau_i)$ is sampled at every $n \times 500$ ($n = 1, 2, \cdots$) MCS. We easily see in Figure 1a that $A(X^2)$ at $\alpha = 1400$ and the one at $\alpha = 1600$ are completely different from each other. This result implies that the convergence speed of our MC on $N = 1500$ fluid surfaces at $\alpha = 1400$ is about 10 times slower than that
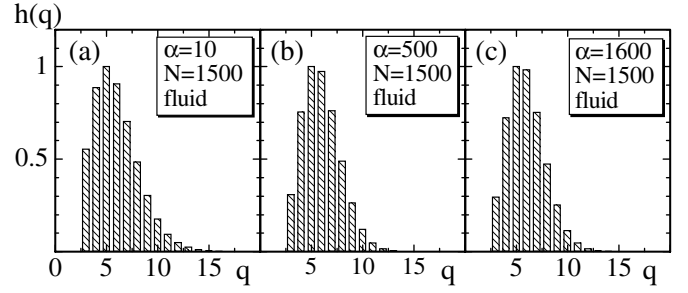

Fig. 2. The normalized histograms $h(q)$ of the coordination number q of the fluid surface of $N = 1500$ at (a) $\alpha = 10$ (crumpled phase), (b) $\alpha = 500$ (branched polymer phase), and (c) $\alpha = 1600$ (smooth phase).

at $\alpha = 1600$, and indicates the existence of some discontinuous phase transition.

The rate of acceptance r_X for X and r_T for bond flip are plotted in Figure 1b. We see in Figure 1b that r_X is almost constant and r_T is discontinuous. In order to maintain $0.5 \leq r_X \leq 0.6$, we adjust ϵ in equation (3) to a suitable value, because r_X rapidly changes against α at the transition point. This is the reason why r_X is not completely constant. The discontinuous behavior of r_T also indicates that the model undergoes a discontinuous transition.

In order to see the distribution of the coordination number q, the normalized histograms $h(q)$ are shown in Figures 2a, b, and c. The histograms $h(q)$ in the figures were obtained in the final 5×10^6 MCS on the fluid surface of $N = 1500$ at (a) $\alpha = 10$, (b) $\alpha = 500$, and (c) $\alpha = 1600$. These three values of α correspond to three distinct phases; the crumpled, the branched polymer, and the smooth phases, which will be clarified later. We note that the coordination number q does not always reach the above mentioned $q_i^{\max}$ the maximum coordination number during the final 5×10^6 MCS in each case. Thus, we find from Figures 2a, b, and c that the coordination number q is dominated by $4 \leq q \leq 7$ at each α in the fluid model. No distinct difference can be seen in $h(q)$ obtained in the three phases, although it can bee seen that $h(q = 3)$ in the crumpled phase at $\alpha = 10$ is larger than those in the other two phases. It is remarkable that $h(q)$ in the smooth phase shown in Figure 2c is almost identical with $h(q)$ in the branched polymer phase shown in Figure 2b, because we expect that the curvature energy S_3 is closely related with the coordination number q and plays an essential role in the phase transition. The variation of q is also very small even at the discontinuous transition point between the branched polymer and the smooth phases.

Nevertheless, we can find in S_3/N a discontinuous change, which reflects a discontinuous transition between the branched polymer and the smooth phases, in both models. However, the gap in S_3/N is very small and comparable with the standard deviation of S_3/N. Hence, we can not conclude only from the gap that the model undergoes a discontinuous transition.

S_1/N vs. b are plotted in Figures 3a and b. We see in Figure 3a that the expected relation $S_1/N = 3/2$ is
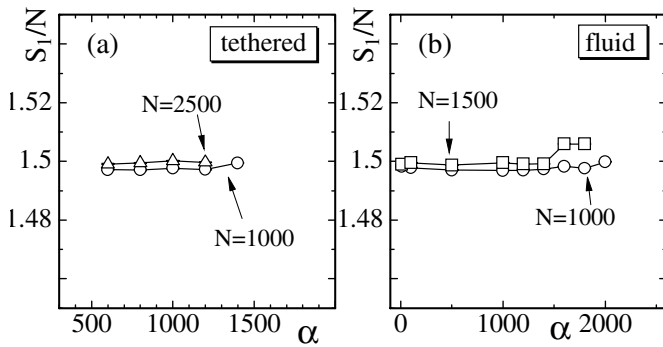
Fig. 3. (a) S_1/N obtained from $N = 1500$ and $N = 2500$ tethered surfaces, and (b) S_1/N obtained from $N = 1000$ and $N = 1500$ fluid surfaces.
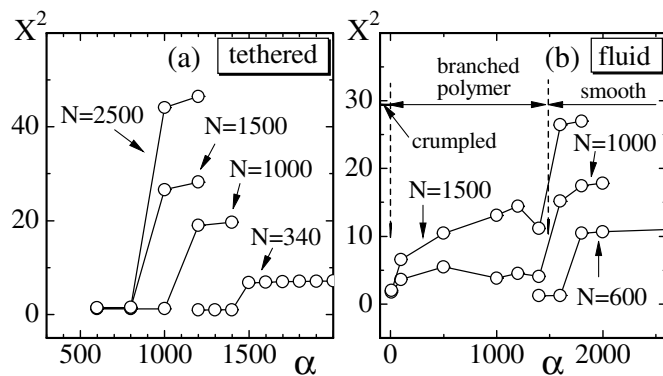

Fig. 4. X^2 vs. α of (a) tethered surface model and of (b) fluid surface model. Dashed lines in (b) denote the phase boundaries on $N = 1500$ fluid surfaces.

satisfied in the tethered model, and also in Figure 3b that $S_1/N = 3/2$ in the fluid model. The discontinuous change seen in S_1/N of $N = 1500$ in Figure 3b implies the existence of a discontinuous transition. Since the gap is almost equal to or less than 0.4% of S_1/N, we consider that the relation $S_1/N = 3/2$ is not influenced by the discontinuous transition. Thus, we understand that the surfaces in both sides of the transition point are in the equilibrium configurations prescribed by Z of equation (1).

The mean square size X^2 is plotted in Figures 4a and b. In the tethered model, X^2 is obtained on surfaces of size up to $N = 2500$. We see a gap in each X^2 in the tethered model. These discontinuous changes of X^2 imply that the phase transition is of first order. On the other hand, the dependence of X^2 on α in the fluid model appears to be continuous on surfaces of $N = 1000$ and $N = 1500$. The reason why X^2 takes intermediate values at α just below the transition point is that the surface belongs to a new phase, which emerges only in the fluid model. This new phase resembles the branched polymer phase [34–36] in shape of the surfaces, which will be shown as a snapshot below. Thus, we call the phase as the branched polymer phase, although we can hardly confirm that the new phase is exactly identical with a branched polymer phase from the present numerical results.

It should also be noted that the fluid surfaces become crumpled when $\alpha \to 0$, as seen in Figure 4b. The

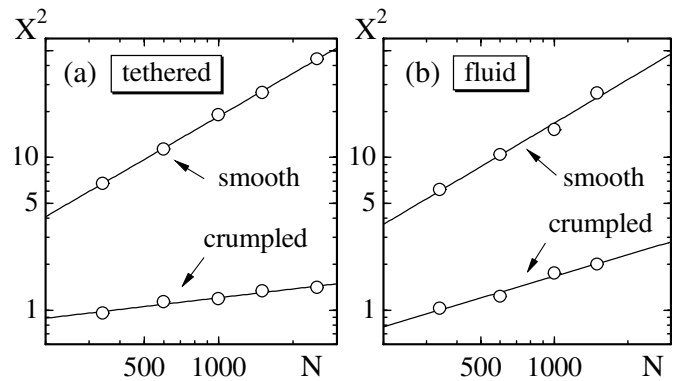**Fig. 5.** X^2 vs. N on (a) tethered surfaces and on (b) fluid surfaces. X^2 denoted by *smooth* in (a) and (b) were obtained in the smooth phase close at the transition point in both models. X^2 denoted by *crumpled* in (a) were obtained just below the transition point. X^2 of surfaces $N \leq 600$ denoted by *crumpled* in (b) were obtained just below the transition point, and those of $N \geq 1000$ were obtained at $\alpha = 10$.

dashed lines drawn vertically in Figure 4b denote the phase boundaries of the fluid surfaces of size $N = 1500$. The leftmost data X^2 in Figure 4b were obtained at $\alpha = 10$ on surfaces of $N = 1000$ and $N = 1500$, and their dependence on N clearly different from those obtained at larger α. Thus, we considered that the phase boundary between the crumpled and the branched polymer phases is located close at $\alpha = 10$.

Figures 5a and b are log-log plots of X^2 against N. X^2 denoted by *smooth* in the figures were obtained in the smooth phase close at the transition point in both models. X^2 denoted by *crumpled* in the tethered model were obtained just below the transition point. X^2 denoted by *crumpled* in the fluid model of $N \leq 600$ were obtained just below the transition point, and those of $N \geq 1000$ were obtained at $\alpha = 10$. The straight lines give the Hausdorff dimension H, which is defined by

$$X^2 \sim N^{\frac{2}{H}}. \tag{6}$$

The surface swells and becomes almost smooth in the smooth phase both in the tethered model and in the fluid model; we already confirmed this from the data in Figures 4a and b. X^2 has a value of the order of the radius squares when the membrane becomes a swollen sphere. Hence, we expect that $H \simeq 2$ in the smooth phase. We have in fact

$$
\begin{aligned}
H &= 2.11 \pm 0.03 \quad (\text{tethered, smooth}), \\
H &= 10.47 \pm 1.23 \quad (\text{tethered, crumpled}), \qquad (7) \\
H &= 1.99 \pm 0.07 \quad (\text{fluid, smooth}), \\
H &= 4.15 \pm 0.47 \quad (\text{fluid, crumpled}).
\end{aligned}
$$

The results in equation (7) obtained in the tethered model indicate that the phase transition between the crumpled and the smooth phases is characterized also by a gap of H. The reason why H is finite in the crumpled phase comes from the fact that X^2 are obtained close at
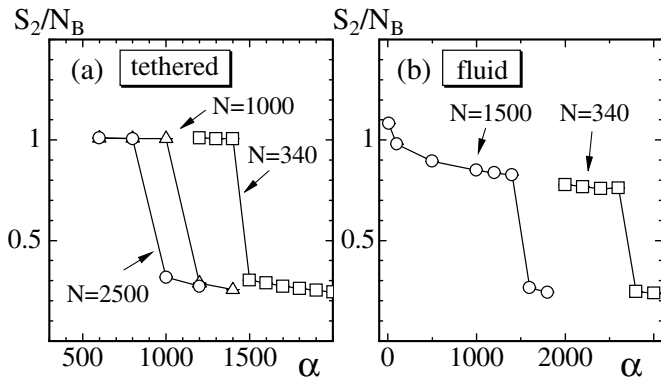
Fig. 6. S_2/N_B vs. b obtained on (a) tethered surfaces and on (b) fluid surfaces. S_2 is defined by $S_2 = \sum_i (1 - \cos \theta_i)$.

Fig. 7. Snapshots of fluid surface obtained in (a) the crumpled phase at $\alpha = 10$, (b) the branched polymer phase at $\alpha = 1200$, and (c) the smooth phase at $\alpha = 1600$. Small spheres represent the vertices. $N = 1500$.

the transition point, which is far distant from $\alpha = 0$, where H is expected to be infinite.

In the fluid model, on the contrary, the dependence of H on α in the branched polymer phase can not be extracted from the present numerical data. In order to see how H depends on α in the branched polymer phase, large-scale simulations are necessary. Nevertheless, it is possible that H continuously changes against α in the fluid model, if the new phase is the branched polymer one. In fact, it is expected that $H \simeq 2$ in the branched polymer phase [34–36]. In addition, we see in Figure 4b that X^2 smoothly changes between the branched polymer phase and the crumpled phase.

Figures 6a and b are the bending energy S_2/N_B vs. α respectively obtained on the tethered surfaces and on the fluid surfaces, where S_2 is defined by $S_2 = \sum_i (1 - \cos \theta_i)$, N_B the total number of bonds. S_2, which is an extrinsic variable and is not included in the Hamiltonian, represents how smooth the surface is. The gap seen in S_2/N_B also indicates that the phase transition is of first order. Thus, we see a first-order transition between the smooth and the crumpled phase in the tethered model, and also see a first-order transition between the smooth phase and the branched polymer phase in the fluid model.

We note that first-order nature of transitions is ordinarily confirmed by a discontinuous change (or a gap) of energy term included in Hamiltonian. A gap in some physical quantity that is not included in Hamiltonian can also confirm loosely a first-order nature of transitions. Thus, we consider that the gap in X^2 in Figures 4a and b, and the gap in S_2 in Figures 6a and b indicate the existence of first order transitions.

Figures 7a, b and c are snapshots of surfaces obtained respectively at the smooth phase, at the branched polymer phase, and at the crumpled phase in the fluid surface model. The tethered surface model gives the same appearance of surfaces as the fluid surface model both in smooth and in crumpled phases, although the tethered model has no branched polymer phase.
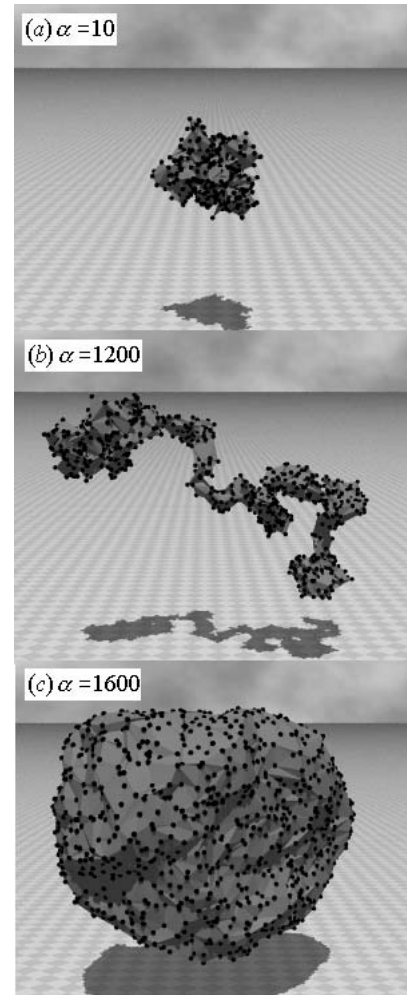
4 Summary and conclusions

We have studied extrinsic properties of surface models of membranes embedded in $\mathbf{R}^3$. The Hamiltonian contains the Gaussian energy term S_1 and the deficit angle term S_3; $S = S_1 - \alpha S_3$. This S_3 was introduced by a straightforward extension of the coordination dependent term, which comes from the weight of the integration measure dX. Two kinds of models were investigated: one is a tethered model and the other is a fluid one. We found in the tethered model that there are two distinct phases; smooth and crumpled, and that these phases are connected by a discontinuous transition. It was also found in the fluid model that there is a new phase (branched polymer phase) between the smooth and the crumpled phases. A discontinuous transition separates the branched polymer phase from the smooth one in the fluid model. Although we called the new phase in the fluid model as the branched polymer phase, large scale simulations are necessary to confirm that the new phase is exactly identical with the branched polymer one.

References

1. A.M. Polyakov, Nucl. Phys. B **268**, 406 (1986)
2. H. Kleinert, Phys. Lett. B **174**, 335 (1986)
3. W. Helfrich, Z. Naturforsch c **28**, 693 (1973)
4. F. David, E. Guitter, Europhys. Lett. **5**(8), 709 (1988)
5. L. Peliti, S. Leibler, Phys. Rev. Lett. **54**, 1690 (1985)
6. M.E.S. Borelli, H. Kleinert, A.M.J. Schakel, Phys. Lett. A **267**, 201 (2000)
7. M.E.S. Borelli, H. Kleinert, Phys. Rev. B **63**, 743 (2001)
8. H. Kleinert, Eur. Phys. J. B **9**, 651 (1999)
9. F. David, *Two dimensional quantum gravity and random surfaces 8*, edited by D. Nelson, T. Piran, S. Weinberg (World Scientific, 1989), p. 81
10. D. Nelson, *Statistical Mechanics of Membranes and Surfaces 5*, edited by D. Nelson, T. Piran, S. Weinberg (World Scientific, 1989), p. 137
11. Y. Kantor, *Statistical Mechanics of Membranes and Surfaces 5*, edited by D. Nelson, T. Piran, S. Weinberg (World Scientific, 1989), p. 115
12. M.J. Bowick, A. Travesset, Phys. Rept. **344**, 255 (2001)
13. K.J. Wiese, *Phase Transitions and Critical Phenomena 19*, edited by C. Domb, J.L. Lebowitz (Academic Press, 2000), p. 253
14. J.F. Wheater, J. Phys. A: Math. Gen. **27**, 3323 (1994)
15. J.F. Wheater, Nucl. Phys. B **458**, 671 (1996)
16. M. Bowick, S. Catterall, M. Falcioni, G. Thorleifsson, K. Anagnostopoulos, J. Phys. I France **6**, 1321 (1996); M. Bowick, S. Catterall, M. Falcioni, G. Thorleifsson, K. Anagnostopoulos, Nucl. Phys. Proc. Suppl. **47**, 838 (1996); M. Bowick, S. Catterall, M. Falcioni, G. Thorleifsson, K. Anagnostopoulos, Nucl. Phys. Proc. Suppl. **53**, 746 (1997)
17. J. Ambjorn, A. Irback, J. Jurkiewicz, B. Petersson, Nucl. Phys. B **393**, 571 (1993)
18. S.M. Catterall, J.B. Kogut, R.L. Renken, Nucl. Phys. Proc. Suppl. B **99A**, 1 (1991)
19. M. Bowick, P. Coddington, L. Han, G. Harris, E. Marinari, Nucl. Phys. Proc. Suppl. **30**, 795 (1993); M. Bowick, P. Coddington, L. Han, G. Harris, E. Marinari, Nucl. Phys. B **394**, 791 (1993)
20. K. Anagnostopoulos, M. Bowick, P. Gottington, M. Falcioni, L. Han, G. Harris, E. Marinari, Phys. Lett. B **317**, 102 (1993)
21. Y. Kantor, D.R. Nelson, Phys. Rev. A **36**, 4020 (1987)
22. G. Gompper, D.M. Kroll, Phys. Rev. E **51**, 514 (1995)
23. H. Koibuchi, Phys. Lett. A **300**, 586 (2002)
24. H. Koibuchi, N. Kusano, A. Nidaira, K. Suzuki, M. Yamada, Phys. Lett. A **319**, 44 (2003)
25. F.F. Abraham, W.E. Rudge, M. Plischke, Phys. Rev. Lett. **62**, 1757 (1989)
26. J.-S. Ho, A. Baumgartner, Phys. Rev. Lett. **63**, 1324 (1989)
27. F.F. Abraham, D.R. Nelson, Science **249**, 393 (1990); F.F. Abraham, D.R. Nelson, J. Phys. France **51**, 2653 (1990)
28. G.S. Grest, J. Phys. France I **1**, 1695 (1991)
29. M. Bowick, A. Cacciuto, G. Thorleifsson, A. Travesset, Eur. Phys. J. E **5**, 149 (2001)
30. C.F. Baillie, D.A. Johnston, Phys. Rev. D **48**, 5025 (1993); C.F. Baillie, D.A. Johnston, Phys. Rev. D **49**, 4139 (1994)
31. C.F. Baillie, D. Espriu, D.A. Johnston, Phys. Lett. B **305**, 109 (1993)
32. C.F. Baillie, A. Irback, W. Janke, D.A. Johnston, Phys. Lett. B **325**, 45 (1994)
33. N. Ferguson, J.F. Wheater, Phys. Lett. B **319**, 104 (1993)
34. H. Koibuchi, A. Nidaira, T. Morita, K. Suzuki, Phys. Rev. E **68**, 011804 (2003)
35. D.M. Kroll, G. Gompper, Science **255**, 968 (1992); D.M. Kroll, G. Gompper, Phys. Rev. A **46**, 3119 (1992)
36. D. Boal, M. Rao, Phys. Rev. A **45**, R6947 (1992)
37. F. David, Nucl. Phys. B **257** [**FS14**], 543 (1985)
38. D.V. Boulatov, V.A. Kazakov, I.K. Kostov, A.A. Migdal, Nucl. Phys. B **275** [**FS17**], 641 (1986)
39. J. Ambjorn, B. Durhuus, J. Frohlich, Nucl. Phys. B **257**, 433 (1985)
40. K. Fujikawa, M. Ninomiya, Nucl. Phys. B **391**, 675 (1993)
41. R. Friedberg, H.C. Ren, Nucl. Phys. B **235** [**FS11**], 310 (1984)